Synthesis by aerosol assisted chemical vapor deposition and microstructural characterization of $PbTiO_3$ thin films

J. Ramos-Cano, A. Hurtado-Macías, W. Antúnez-Flores, L. Fuentes-Cobas, J. González-Hernández, P. Amézaga-Madrid, M. Miki-Yoshida

Abstract

Thin films of $PbTiO_3$ were deposited onto (001) silicon single-crystal substrates by aerosol assisted chemical vapor deposition method at different temperatures, using organometallic precursors. With the objective of stabilizing and homogenizing the perovskite phase, the films were annealed at 800 °C, in a Pb-rich atmosphere, for 4 and 6 h. The evolution of compositions and microstructure of the films was characterized before and after annealing, by grazing incidence X-ray diffraction, two-dimensional detection of grazing incidence diffraction with synchrotron radiation, scanning electronmicroscopy and high resolution transmission electron microscopy. X-ray diffraction results showed that the crystalline structure of optimized $PbTiO_3$ films corresponded to a tetragonal perovskite-type, with lattice parameters a=0.387(4)nmand c=0.406(4)nm. In addition, the inverse pole figure of the fiber texture representation, had a Gaussian (1, 1, 0) component and distribution width Ω=15°.

Keywords: Ferroelectrics, Aerosol-assisted chemical vapor deposition, Lead titanate, Thin films, X-ray diffraction, Scanning electron microscopy, Transmission electron microscopy.

Introduction

With the development of microelectronic technology, the performance requirement of ferroelectric thin films increased. Lead-based ferroelectric thin films had been used lately in the electronic industry due to their easy integration in electronic or optoelectronic devices such as: piezoelectric transductors, non-volatile memory, infrared detectors, and high-sensibility pyroelectric sensors [1–11]. Lead titanate (PT) is not an exception, with its Perovskite type structure and singular properties such as spontaneous polarization, a high Curie temperature (490 °C), a large tetragonality, a relatively low permittivity, and a large pyroelectric coefficient [12,13]. These properties make this material a good candidate for use in the electronic industry, as a promising ferroelectric material. Several methods, physical and chemical, are utilized to deposit ferroelectric PT thin films including sol–gel and hydrothermal methods [14], radiofrequency magnetron sputtering [15], pulsed laser ablation [16] and chemical vapor deposition (CVD) [17,18]. There are a fewstudies of PT synthesis by CVD method, including aerosol assisted chemical vapor deposition (AA-CVD) technique. AA-CVD represents a good route to the synthesis of thin films, and it has been proved to be a simple, reproducible and inexpensive method to produce metallic oxide films, representing a great advantage in installations at an industrial level [19–21]. In this variant of the CVD method the precursor transport towards the substrate is performed by means of a carrier gas and an aerosol. The aerosol was obtained by atomization of a precursor solution containing the element of interest. The carrier gas can be inert or oxidant. This technique is similar to atmospheric pressure CVD, metal organic CVD, spray pyrolysis, chemical spray, pyrosol, etc. The principal difference between spray

variants and AA-CVD is that in the latter the precursor arrives into contact with the substrate's surface in gas phase; the synthesis parameters must be optimized to achieve this condition. The deposition rate, composition, thickness, microstructure and other important parameters of the films can be easily controlled.

This work presents the synthesis of $PbTiO_3$ films onto (001) silicon substrates, by the AA-CVD method. PT films were annealed to obtain the perovskite phase. The microstructure of the films was characterized before and after annealing, by grazing incidence X-ray diffraction (GIXRD), two-dimensional detection of grazing incidence diffraction (2D-GIXRD) with synchrotron radiation, scanning electronmicroscopy (SEM) and high resolution transmission electronmicroscopy (HRTEM). The crystalline phases, composition, morphology, and other relevant properties of the PT thin films were discussed in correlation to the deposition and processing parameters.

Experimental methodology

$PbTiO_3$ thin films were deposited onto (001) silicon substrates (2.5×2.5 cm2) by the AA-CVD technique; details of the experimental set-up have been described before [22,23]. The starting solution was a dilution of lead acetate (II) tri-hydrate [$Pb(C_2H_3O_2)_2$ $3H_2O$] and titanium (IV) oxyacetylacetonate [$(C_5H_8O_2)_2$ TiO] in methanol (99.9%).

Table 1
Optimized deposition conditions of samples PT1, PT2 and PT3 onto Si substrates.

Sample	Deposition temperature (°C)	Solution concentration ($mol \cdot dm^{-3}$)		Carrier gas flux ($L\ min^{-1}$)	Distance nozzle–substrate (mm)	Velocity of nozzle ($cm\ min^{-1}$)
		Ti	Pb			
PT1	350	0.025	0.025	4	2	1
PT2	375					
PT3	400					

Solution homogeneity was assured by stirring in a magnetic agitator at 950 rpm and room temperature, for 1 h. Before use, the substrates were washed sequentially in acetone, methanol and tri-distilled water in an ultrasonic bath, for 10 min in each solvent. Several preliminary optimization tests were performed to fix other deposition parameters, such as concentration of the starting solution, carrier gas flux, nozzle substrate distance, etc. After the initial optimization tests the films were synthesized with the deposition conditions shown in Table 1; the only variable was substrate temperature. In this report, 3 samples (PT1, PT2, and PT3)were deposited at 350, 375 and 400 °C, respectively. The aerosol was generated by a Sonaer 241 PG ultrasonic nebulizer operated at 2.4 MHz. It was carried by micro-filtered air; handled at the optimized pressure of 310 kPa and flux of 5 L min^{-1}. Then, the aerosol was directed towards the substrate by a nozzle, which had a periodic movement at a constant velocity of 1 cm·min^{-1} to deposit uniform films onto the greater part of the substrate's surface.

Samples were annealed at 800 °C for 4 and 6 h, in a Lindberg/Blue M tubular furnace, model STF54454C. A Pb-rich atmosphere was used, by placing PbO powder around the samples. Five segmentswere applied to stabilize the ferroelectric perovskite phase (see Fig. 1). Segments 1 and 2 were used to decompose and eliminate possible organic residues from the precursor. Steps 3 and 4 correspond to the high temperature annealing. The heating and cooling ratewas 3 °C min^{-1}. Eachdeposited sample was cut into four equivalent sections, to perform different annealing tests.

The surface morphology and cross sectional microstructure of the films were studied by field emission scanning electron microscopy using a JEOL JSM-7401F operated at 7 kV. SEM images were obtained in secondary and backscattered electron image modes. Cross sectional studies were performed to determine their thickness. In addition, elemental analysis of the filmswas achieved bymeans of energy dispersive X-ray spectroscopy (EDS), using an Oxford Inca microanalysis system attached to an electron microscope, with 100 s of live time acquisition and 5 eV/ch of energy dispersion. High-resolution transmission electron microscopy of the cross section of the films was performed in a JEOL JEM-2200FS system operated at 200 kV. Samples for HRTEM were prepared using a JEOL JEM-9320 focused ion beam system operated at 30 kV, with Ga ions.

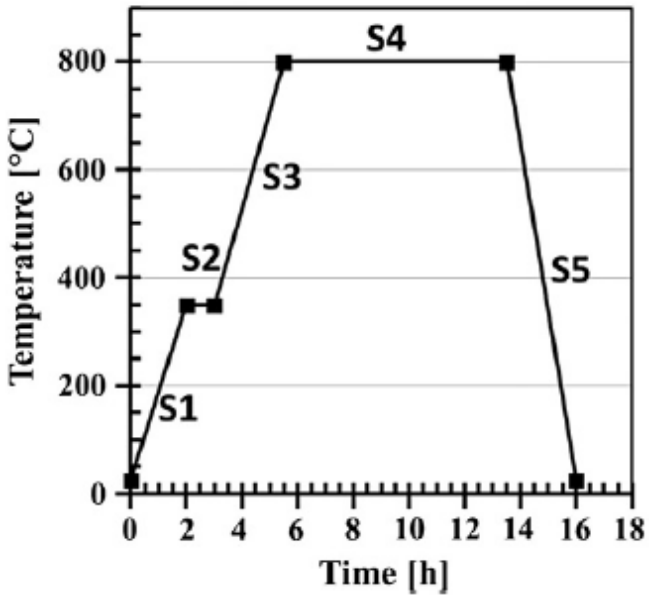

Fig. 1. Temperature ramp of the thermal treatment performed to PT films.

The crystalline structure of the samples was analyzed by grazing incidence XRD in a Panalytical X-Pert system, and the patterns were obtained using Cu Kα radiation at 40 kV and 35 mA. A diffracted beam path included a graphite flat crystal monochromator. The grazing incidence angle was fixed at 0.5°;whereas the scanning angle 2θ was varied between 20° and 60°, at a 0.02° step size. Selected samples were investigated by two-dimensional detection of grazing incidence XRD at beamline 11-3 of the Stanford Synchrotron Radiation Lightsource. The characteristic parameters of the 2D-GIXRD experiment were: λ=0.97440 Å, 2D-detector mar345 (diameter=345 mm), sample to detector distance of 150 mm, screen pixel dimensions of 0.15× 0.15 mm^2 and incidence angle=0.3°. A LaB6 standard was used to calibrate the 2D-GIXRD experiment and to evaluate the instrumental peak broadening.

Results and discussion

Crystalline structure: X-ray diffraction patterns of as deposited samples PT1 and PT2, corresponding to low-temperature depositions, did not show welldefined diffraction peaks. These samples consisted, essentially, of amorphous films. Fig. 2 shows the GIXRD patterns of sample PT3, deposited at 400 °C. Plot a), of the as deposited film, shows small broad diffraction peaks corresponding to incipient crystallization of the film. Annealed sample PT3 at 800 °C during 4 and 6 h leads to XRD patterns b) and c), respectively. Crystallization of the $PbTiO_3$ phase is apparent [24]. Diffraction patterns corresponding to the 6 h treatment, present a couple of interesting characteristics: i) peak positions are slightly displaced to the low-d side, as compared with bulk $PbTiO_3$, indicating that a deformation of the primitive structure is present, probably due to a

stress generated during the synthesis or annealing; ii) (100) peak intensity is higher than twice the (001) peak intensity, so a certain texture is present. Fig. 3(a) shows the 2D-GIXRD pattern of sample PT3, obtained with synchrotron radiation. Debye rings of tetragonal $PbTiO_3$ phase with fiber texture can be observed. Computer simulation of this pattern, performed using the program ANAELU [25], allows a detailed interpretation of the considered sample crystal structure and texture.

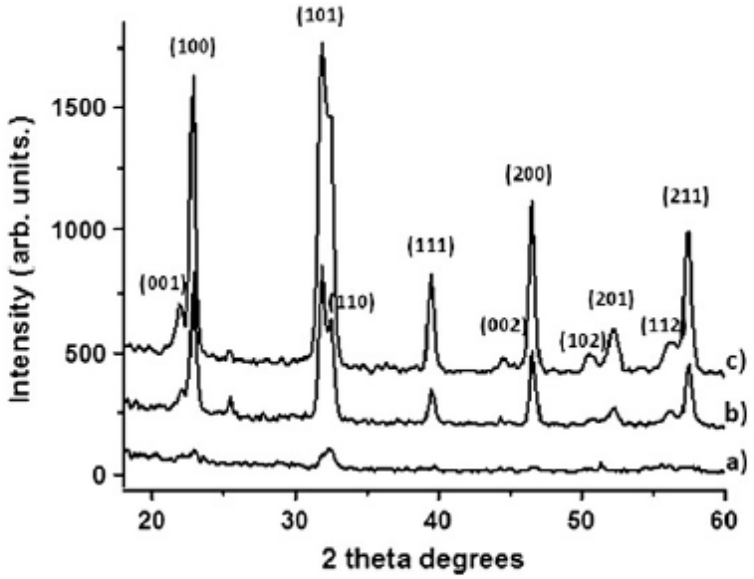

Fig. 2. Evolution of GIXRD patterns for sample PT3 with annealing. a) Before annealing; b) after 4 h at 800 °C; c) after 6 h at 800 °C.

Calculated 2D-GIXRD is represented in Fig. 3(b). Fig. 3(c) characterizes the inverse pole figure associated with the fiber axis of the proposed texture [26]. Peak broadening, in GIXRD as well as in 2D-GIXRD experiments, comprehend instrumental, small crystal size and strain contributions. To estimate strain effects, instrumental and crystal size contributions were determined by independent measurements. Evaluation of

strain broadening allowed assessing that physical variations of the PbTiO3 lattice parameters were of the order of 1%. The final characterization of the sample structure and microstructure, consistent with Figs. 2(c) and 3(a), (b) and (c), is as follows:

– Crystal structure: tetragonal $PbTiO_3$, space group P4mm

– Lattice parameters: a=0.387(4)nm and c=0.406(4)nm

– Fiber texture representation: inverse pole figure with a Gaussian

(1, 1, 0) component, distribution width Ω=15°.

Morpholoygy, composition and microstructure of the films: The perovskite phase evolution can be improved by two factors: i) deposition temperature, and ii) thermal treatment. It is well known that an appropriate thermal treatment improves the perovskite phase homogeneity [20,21,27], even though only fewworks [19] had reported the correlated influence of both deposition temperature and annealing time. Our results suggest that an optimum deposition temperature favored the nucleation and enlargement of the pyrochlore phase, which acts as the precursor of the perovskite phase.

SEM images of as deposited PT1 and PT2 samples show that they had smooth, crack-free surfaces (Fig. 4a and b). Sample PT3 deposited at 400 °C (Fig. 4c), presents morphological features characteristic of crystalline grains; indicating that the deposition temperature was adequate to initiate precursor reaction on the substrate's surface. Microstructural evolution of existent phases was, in general, more evident with the increase of deposition temperature, since nucleation centers had a greater development to promote phase stabilization.

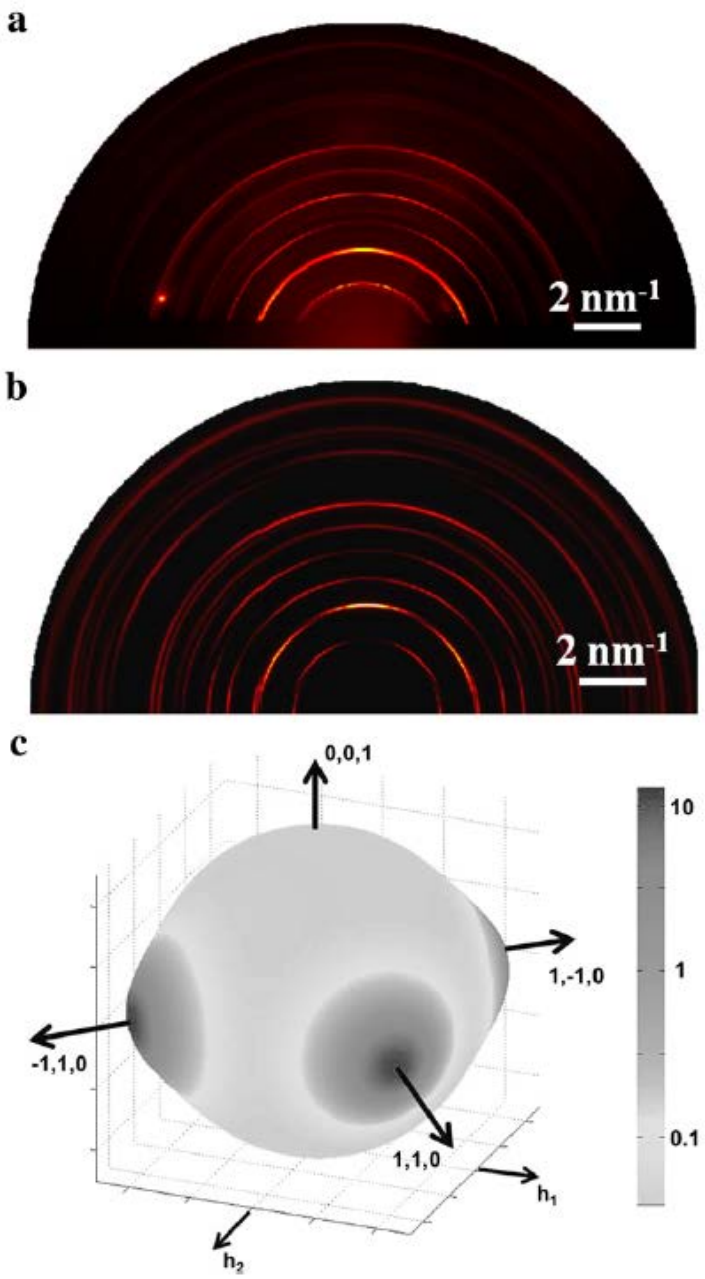

Fig. 3. a) Experimental 2D-XRD pattern of sample PT3. Non-uniform distribution of intensities along the Debye rings demonstrates the presence of a crystallographic texture. b) Computer simulated 2D-XRD of a $PbTiO_3$ thin film showing a fiber texture with (1, 1, 0) inverse pole figure, and distribution width $\Omega = 15°$. The simulated pattern shows the fundamental features of the observed pattern in (a). c) Inverse pole figure of the annealed $PbTiO_3$ thin film PT3 (the plot was performed using the program SAMZ [291]).

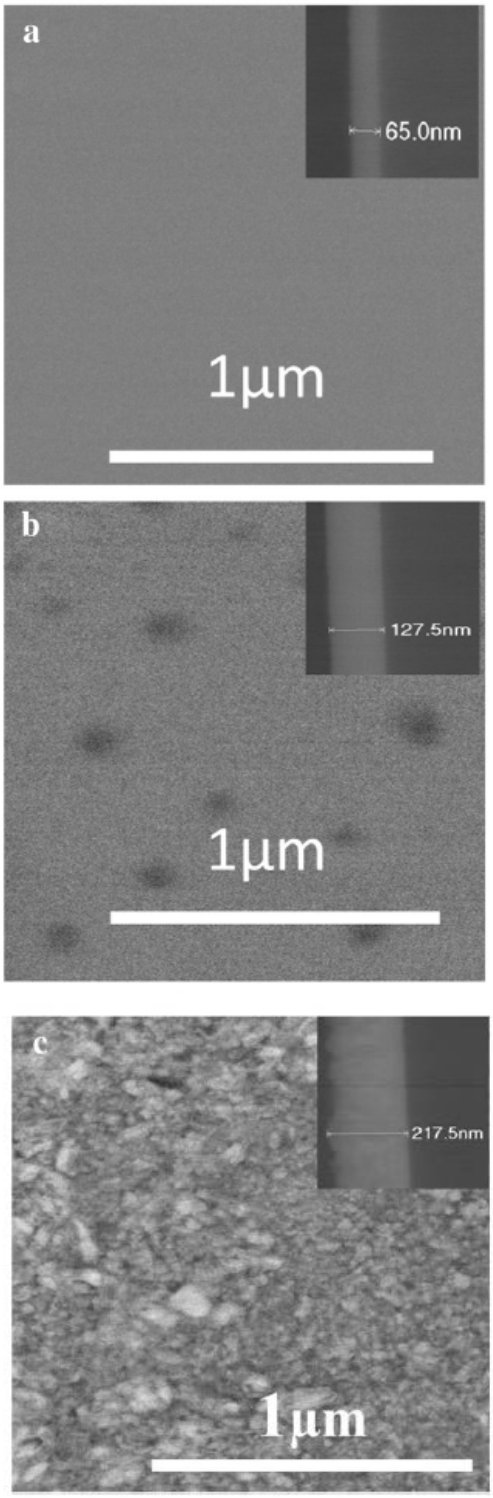

Fig. 4. SEM micrographs of the surface morphology of samples a) PT1, b) PT2 and c) PT3. The insets show the cross section of the films.

Additionally, satisfactory EDS microanalysis was observed, related to the necessary proportion between Ti and Pb atoms. In conclusion, the best result was found in sample PT3.

On the other hand, SEM images of the samples after annealing showed homogenous films (Fig. 5) composed of grains of $PbTiO_3$ and other oxides. When the annealing time was increased, grains increased (main perovskite phase), while the other phases decreased or disappeared. The optimum results were obtained, for samples PT2 and PT3, with an annealing time of 6 h; where the grains showed characteristic ferroelectric domains of the perovskite phase (see Fig. 5c). The average grain size was 84 nm, for the annealed films (Fig. 5b and c), which is independent of the annealing time and in accord with other reports [28]. The development of the perovskite phase is consistent with the fact that the transition process was thermally activated [29,30].

EDS concentrations of Pb and Ti in the non-annealed samples were higher as the deposition temperature increased; this behavior is consistent with the increase in film thickness (see Table 2 and Fig. 4). In addition, a sharp decrease of the Pb concentrations was determined after the first 4 h of annealing (see Table 2); this diminution can be attributed to changes in the microstructure, principally by the re-evaporation and diffusion into the substrate, as discussed below. For the higher annealing time (6 h), the lead concentration remained practically constant. Ti concentration suffers a slight decrease, consistent with the decrease of the film thickness.

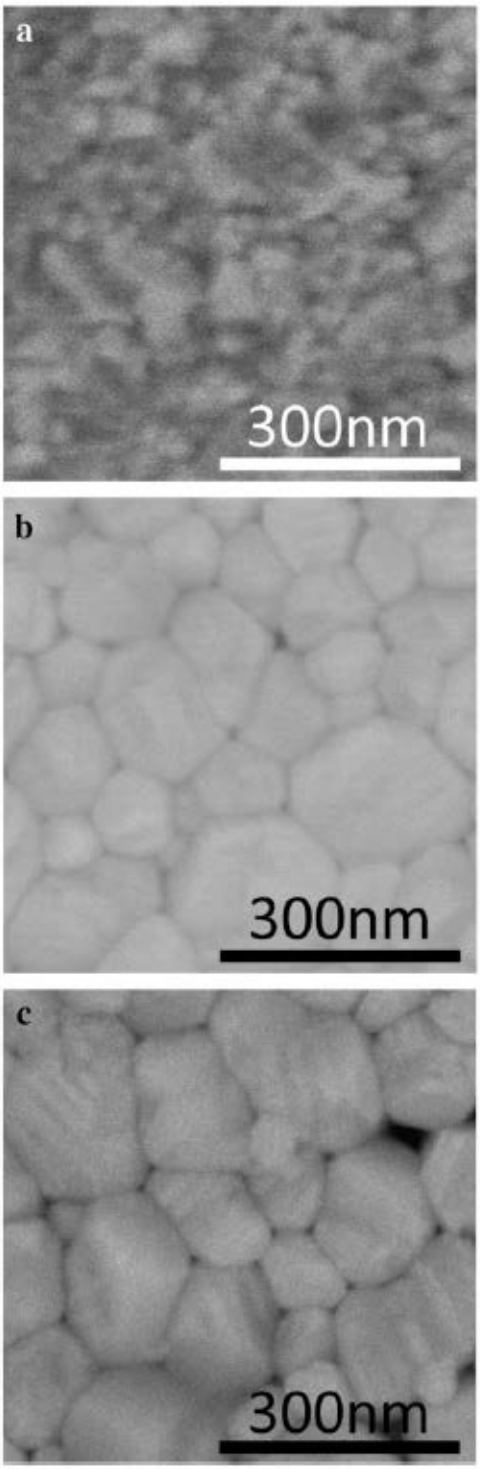

Fig. 5. SEM micrographs of sample PT3 showing its microstructural evolution of the surface of the film, before and after thermal treatment at 800 °C. a) Before annealing, b) annealed for 4 h and c) annealed for 6 h.

Fig. 6 shows TEM images of the cross section of sample PT3 subjected to different annealing times. The evolution of the perovskite phase for this film as a function of the annealing time (0, 4 and 6 h) is shown. The as deposited sample presents a uniform microstructure (Fig. 6a), consistent with the surface morphology observed in the SEM analysis. In contrast, the cross section of the PT3 film annealed for 4 h, presented discrete portions of high Ti and others of high Pb contents (Fig. 6b). When the annealing time was increased to 6 h, the PT3 film was more homogenous in the development of the perovskite phase (Fig. 6c). The films' thickness diminished systematically during the thermal treatment of the PT3 sample; from 220±25 nm for the non-annealed film to 202±15 nm and 180±6 nm for the 4 and 6 h annealed films, respectively. In addition, sample roughness diminished, as indicated by the standard deviation of the thickness.

An interesting trend was observed in the annealed samples. At the bottom of the film, near the interface with the substrate, small globular precipitates (10–40 nm) of lead oxide were formed during the annealing. These precipitates, which are positioned very close to the abrupt SiO_2/Si interface, and detached (40–70 nm) from the bottom of the film (see Fig. 7b and c), are immersed in a SiO_2 layer. Despite the assumption that the thickness of the SiO_2 layer (around 110 nm) was independent of the annealing time, the size and depth of the precipitates change, becoming smaller (9 to 27 nm) and closer (20 nm) to the SiO_2/Si interface for longer annealing times. The interpretation of this phenomenon cannot be done by considering only the inter-diffusion of Si, O and Pb. It is well known that the addition of lead oxide to glass reduces its viscosity, rendering it

almost 100 times more fluid than an ordinary soda glass above the softening temperature (about 600 °C). The complete mechanism is not yet understood; but it could be related to the inter-diffusion of Si, O, and Pb, the formation of a mixed Si–Pb oxide layer of low viscosity, which grows and propagates, below the film during the annealing, and finally to the precipitation of the globular lead oxide nanoparticles, as the temperature decreased. All these Si–Pb oxide mediated processes occur at the same time as lead evaporation, crystallization of the perovskite phase and densification in the upper deposit of the film, leading to the microstructure observed in Fig. 7. It is worthwhile to mention that the film's surface roughness is lower than that of the film–substrate interface, which is a consequence of the Si–Pb oxide layer formation and evolution, as mentioned previously.

Table 2
Variation of the elemental concentration (EDS) and thickness of the films PT1, PT2 and PT3, before and after thermal treatment at 800 °C. As a reference, the measured Si concentration of the substrate is shown.

Sample	Deposition temperature (°C)	Annealing time (h)	Elemental concentration (at.%)			Thickness (nm)
			Si	Ti	Pb	
PT1	350	0	51.9	4.5	8.0	57 ± 7
		4	64.3	1.7	0.8	80 ± 16
		6	43.9	12.0	0.7	105 ± 11
PT2	375	0	26.9	10.1	11.1	127 ± 3
		4	55.0	3.0	2.0	138 ± 8
		6	49.4	4.7	3.1	152 ± 9
PT3	400	0	3.0	14.7	12.0	220 ± 25
		4	19.7	9.8	8.7	202 ± 15
		6	23.9	10.9	10.1	180 ± 6

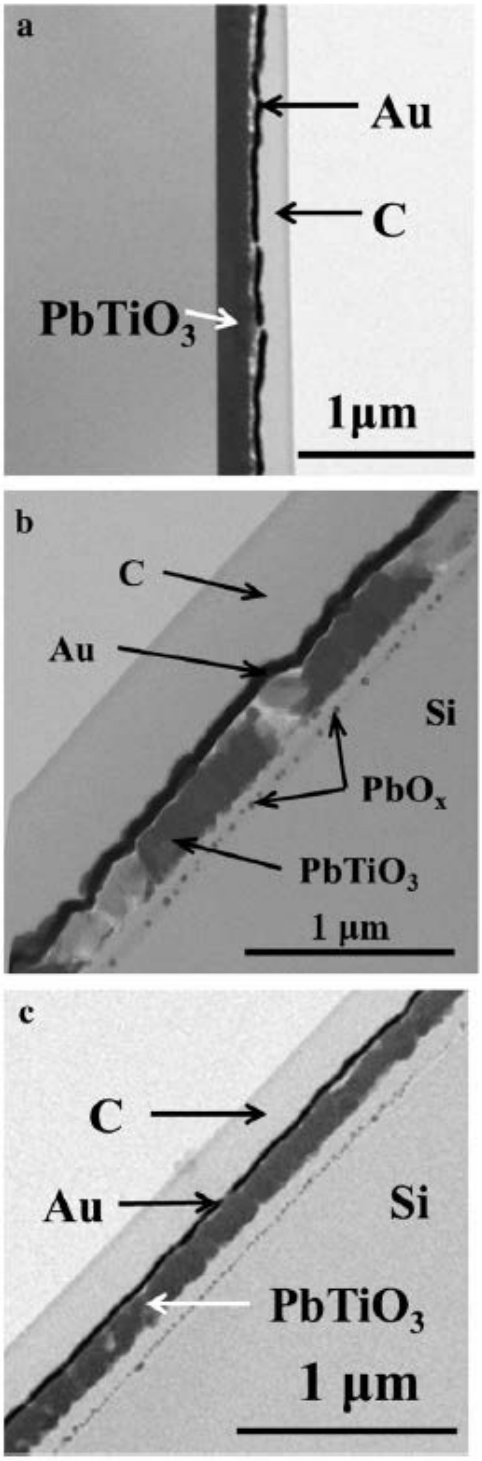

Fig. 6. Low magnification bright field STEM micrographs of the cross section of sample PT3 subjected to different annealing times at 800 °C. a) Before annealing, b) annealed for 4 h and c) annealed for 6 h. Layers of Au and C were deposited for protection of the film's surface in the TEM cross section sample preparation.

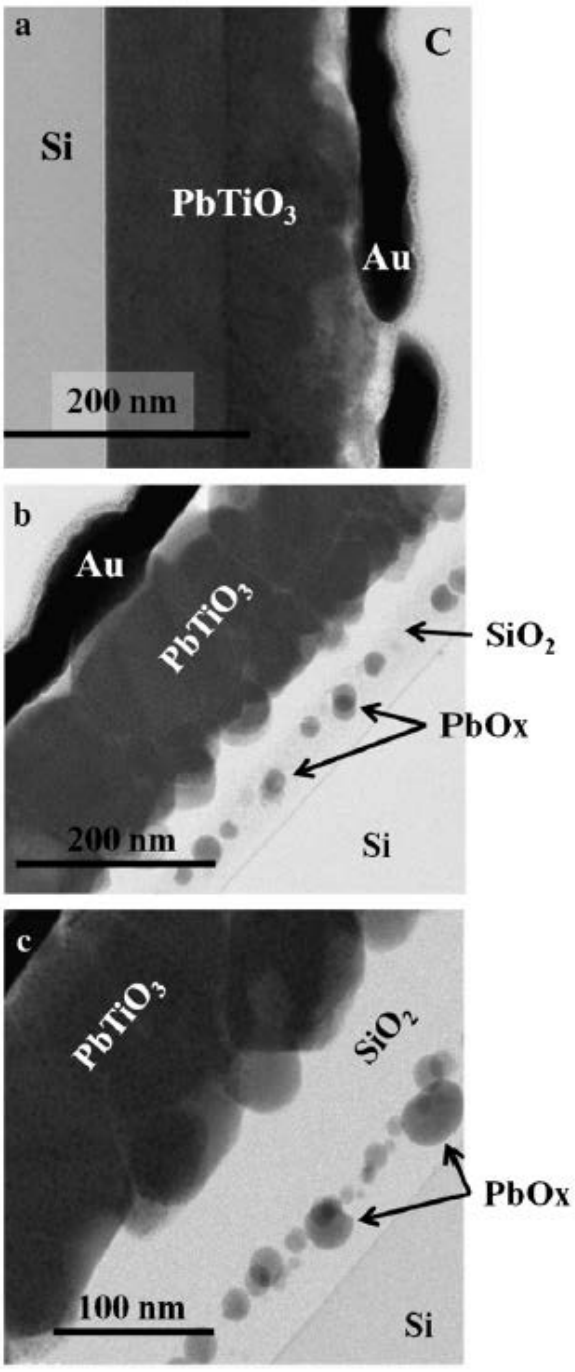

Fig. 7. High resolution STEM images of the cross section of sample PT3 showing precipitates of lead oxide and different layers formed during annealing, due to the Pb and Si inter-diffusion. a) Before annealing, b) annealed for 4 h and c) annealed for 6 h. Layers of Au and C were deposited for protection of the film's surface in the TEM cross section sample preparation.

A cross sectional HRTEM micrograph of sample PT3 annealed at 800 °C for 6 h (Fig. 8a) shows well crystallized, very uniform and homogeneous $PbTiO_3$ films at the nanometric level; i.e. with similar elemental analysis, morphology and crystalline structure. The nanobeam diffraction pattern displays high intensity diffracted spots; which match with zone axis [111] of the perovskite tetragonal structure (see inset). Fig. 8b shows the simulated diffraction pattern that corresponds to the [111] zone axis [31].

Conclusions

High quality, uniform, homogeneous and well adhered $PbTiO_3$ thin films, with a perovskite-type structure, were obtained onto Si substrates by the aerosol assisted CVD technique, followed by a thermal treatment at 800 °C.

2D-GIXRD results showed that the crystalline structure of the $PbTiO_3$ film corresponded to a tetragonal perovskite-type, with lattice parameters a=0.387(4)nm and c=0.406(4)nm. In addition, the inverse pole figure of the fiber texture representation, had a Gaussian (1, 1, 0) component and distribution width Ω=15°.

The optimum and most relevant conditions to stabilize and improve the homogeneity of the perovskite phase were: precursor solution of equal concentration (0.025 $mol \cdot dm^{-3}$) of Ti and Pb; adequate solution homogenization; deposition temperature of 400 °C and annealing at 800 °C for 6 h.

Phases of Pb and Ti oxides inserted in the pyrochlore matrix were observed as the predecessors of the perovskite phase. These phases were observed only for films deposited at 400 °C. Subsequent annealing of the films, at the optimum conditions, followed two distinctive processes. First, close to the surface of the film,where Pb

evaporation, crystallization of the $PbTiO_3$ perovskite phase, and its densification caused the final microstructure of the film. Second, near the film–substrate interface, where the Si–Pb oxide layer of low viscosity produced the lead oxide nanoparticles immersed in the thick SiO_2 layer.

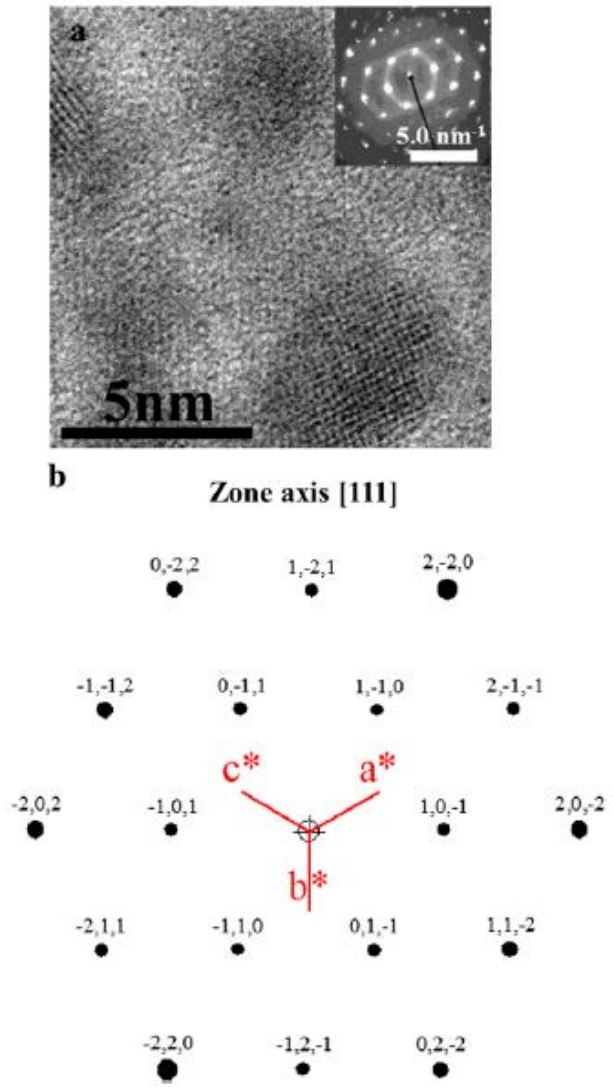

Fig. 8. a) HRTEM micrograph of sample PT3. The inset shows the nano-beam diffraction pattern of the same zone. b) Simulated diffraction pattern for sample PT3 annealed at 800 °C for 6 h.

Acknowledgments:

The authors thank O. Solis, C. Ornelas, C. Leyva, S. Miranda, M. Moreno, A. Rubio and E. Torres for their technical support. 2D-GIXRD was carried out at the Stanford Synchrotron Radiation Laboratory, a national user facility operated by Stanford University on behalf of the U.S. Department of Energy, Office of Basic Energy Sciences. Financial support from CONACyT (Project 102181) and SEP-CONACYT project no 2008-1-106655 is gratefully acknowledged.

References

[1] Ch. Dyun, J.W. Jang, Y.J. Chao, K. Jai Lee, B.W. Lee, Thin Solid Films 324 (1998) 94.

[2] H. Huang, X. Yao, X. Wu, M. Wang, L. Zhang, Microelectron. Eng. 66 (2003) 688.

[3] A.R. Raju, C.N.R. Rao, Appl. Phys. Lett. 66 (1995) 896.

[4] M. Tong, G. Dai, D. Gao, Mater. Lett. 46 (2000) 60.

[5] Ch.Ch. Chan, Thin Solid Films 311 (1997) 304.

[6] J.R. Soh, H.M. Lee, H.S. Kwon, Calphad 18 (1994) 237.

[7] D. Bao, X. Yao, N. Wakiya, K. Shinozaki, N. Mizutani, Mater. Sci. Eng. B94 (2002) 269.

[8] Ch. Byun, J.W. Jang, B.W. Lee, Mater. Lett. 34 (1998) 308.

[9] D. Bao, X. Yao, K. Shinozaki, N. Mizutani, J. Cryst. Growth 259 (2003) 352.

[10] In: K. Uchino, M. Dekker, Inc. (Eds.), Ferroelectric Devices, New York, 2000.

[11] Y. Ya, T. Ski, L.F. Rybakova, T.V. Lunina, O.F. Fedoseeva, S.G. Prutchenko, S.A. Ment'shikh, Inorg. Mater. 37 (2001) 500.

[12] J. Harjuoja, A. Kosola, M. Putjonen, L. Niinisto, Thin Solid Films 496 (2006) 346.

[13] Y.I. Park, C.E. Kim, H.W. Lee, J. Sol-Gel Sci. Technol. 14 (1999) 149.

[14] D.G. Wang, C.Z. Chen, J. Ma, T.H. Liu, Appl. Surf. Sci. 255 (2008) 1637.

[15] Z. Xu, W. Chan, Acta Mater. 55 (2007) 3923.

[16] M. Lisca, L. Pintilie, M. Alexe, C.M. Teodorescu, Appl. Surf. Sci. 252 (2006) 4549.

[17] K. Byun, W. Lee, Curr. Appl. Phys. 7 (2007) 113.

[18] J.M. Koo, S. Kim, S. Shin, Y. Park, J.K. Lee, Ceram. Int. 34 (2008) 1003.

[19] P.S. Patil, Mater. Chem. Phys. 59 (1999) 185.

[20] D. Perednis, L.J. Gauckler, J. Electroceram. 14 (2005) 103.

[21] K.L. Choy, Prog. Mater. Sci. 48 (2003) 57.

[22] P. Amézaga-Madrid,W. Antúnez-Flores, I. Monárrez-García, J. González-Hernández, R. Martínez-Sánchez, M. Miki-Yoshida, Thin Solid Films 516 (2008) 8282.

[23] P.Amézaga-Madrid,W. Antúnez-Flores, J. González-Hernández, J. Sáenz-Hernández, K. Campos-Venegas, O. Solís-Canto, C. Ornelas-Gutiérrez, O. Vega-Becerra, R. Martínez-Sánchez, M. Miki-Yoshida, J. Alloys Compd. 495 (2010) 629.

[24] Joint Committee on Powder Diffraction Standards, Powder Diffraction File, International Center for Diffraction Data, Swarthmore, PA, 2006. (cards 01-078-0299).

[25] L. Fuentes-Montero, M.E. Montero-Cabrera, L. Fuentes-Cobas, J. Appl. Crystallogr. 44 (2011) 241.

[26] A.Muñoz-Romero, G. Aquino-De Los Ríos, P. Domínguez-Barrera, L. Fuentes-Montero, J. Camarillo-Cisneros, H. Camacho-Montes, M.E. Fuentes-Montero, M.E.

Montero- Cabrera, M. García-Guaderrama, L. Fuentes-Cobas, Integr. Ferroelectr. 125 (2011) 61.

[27] M. Cruz, L. Hernán, J. Morales, L. Sánchez, J. Power Sources 108 (2002) 35.

[28] Ch.K. Kwok, S.B. Desu, L. Kammerdiner, Mater. Res. Soc. Symp. Proc. 200 (1990) 83.

[29] J.A. Voigt, B.A. Tuttle, T.J. Headley, M.O. Eatough, D.L. Lamppa, G. Goodnow, Mater. Res. Soc. Symp. Proc. 310 (1993) 15.

[30] C.G. Levi, Acta Mater. 46 (1998) 787.

[31] U.S. National Institute of Standards, Technology, FachinformationszentrumKarlsruhe, Germany and the U.S. Department of Commerce on the behalf of the United States. Inorganic Crystal Structure Database — ICSD, Version 1.7.1 2010-2.